Kinetic Studies of Oxygen Reactivity in Soybean Lipoxygenase-1†

Michael J. Knapp‡ and Judith P. Klinman*

Department of Chemistry and Department of Molecular and Cell Biology, University of California, Berkeley, California 94720

Received April 14, 2003; Revised Manuscript Received July 7, 2003

ABSTRACT: The reactivity of O_2 with soybean lipoxygenase-1 (SLO) has been examined using a range of kinetic probes. We are able to rule out diffusional encounter of O_2 with protein, an outer-sphere electron transfer to O_2, and proton transfer as rate-limiting steps in $k_{cat}/K_M(O_2)$ for wild-type enzyme (WT SLO); this restricts the rate-limiting step to either the combination of O_2 with $L^{\bullet}$ or a subsequent conformational change. In the $Ile^{553} \rightarrow$ Phe mutant, which constricts the putative O_2 binding channel [Knapp et al. (2001) *J. Am. Chem. Soc. 123*, 2931−2932], $k_{cat}/K_M(O_2)$ decreases by over a factor of 20; yet, this mutant appears to have the same rate-limiting step as WT SLO. It is argued that the slow step on $k_{cat}/K_M(O_2)$ is the combination of O_2 with $L^{\bullet}$, with proximal protein effects determining the rate of reaction. The available data for SLO support the view that enzymes can affect O_2 reactivity without a direct involvement of metal cofactors. The primary role of the Fe^{3+} cofactor is to generate an enzyme-bound radical, while the protein is concluded to control the stereo- and regiochemistry of O_2 encounter with this radical.

Lipoxygenases (LOs) use O_2 to oxidize polyunsaturated fatty acids into fatty acid peroxides (*1*), which in turn are converted into important physiological regulators such as leukotrienes and lipoxins (*2*). Oxidative stress and carcinogenesis are associated with uncontrolled LO activity, making these enzymes important pharmaceutical targets (*2*, *3*). LOs generate a carbon-centered radical during turnover, yet the reaction with O_2 typically exhibits high regio- and stereospecificity (*4*−*6*). Little has been known regarding how LOs control this biradical combination between $^3O_2$ and $^2L^{\bullet}$. The subject of this study is a detailed analysis of the oxidative chemistry of soybean lipoxygenase.

Soybean lipoxygenase-1 (SLO)[1] has high sequence identity with all mammalian LOs, and its X-ray crystal structure reveals similar structural details (*7*, *8*). For this reason, SLO is commonly used as an analogue of the mammalian enzymes, due to both the availability of a high-yield bacterial expression system (*9*) and the ease of enzyme isolation (*10*). The X-ray crystal structure of SLO reveals many solvent-filled cavities, one of which (cavity IIa) has been demonstrated to impact fatty acid binding in mammalian lipoxygenases (*11*−*15*). This substrate-binding cavity terminates near the protein surface at Lys^{260} and extends to the vicinity of the Fe^{3+}−OH in the active site. A side channel intersects cavity IIa between residues Ile^{553} and Trp^{500}, with constrictions due to Val^{564} and Ile^{553} and a branch toward the surface near residues Pro^{204} and Arg^{203} (*7*).

SLO follows an ordered bi−uni kinetic mechanism, in which linoleic acid (LA) reacts initially, followed by O_2, with subsequent release of product [13-(*S*)-hydroperoxyoctadecadienoic acid [13-(*S*)-HPOD]] (*16*). The reaction with LA is an irreversible $H^{\bullet}$ abstraction (*16*) by the active site Fe^{3+}−OH (*17*, *18*) to generate linoleyl radical ($L^{\bullet}$) and reduced enzyme ($Fe^{2+}-OH_2$). Formation of the radical intermediate ($L^{\bullet}$) is rate-limiting under conditions of substrate saturation (*19*). In the absence of O_2, this intermediate accumulates and can be spectroscopically observed either by loss of the UV absorption characteristic of the Fe^{3+} oxidation level (*20*) or by the appearance of an EPR signal due to the linoleyl radical (*21*). O_2 rapidly reacts with this radical to form product [13-(*S*)-HPOD] and regenerate oxidized enzyme (Fe^{3+}−OH).

The irreversible $H^{\bullet}$ abstraction kinetically separates overall catalysis by SLO into reductive and oxidative half-reactions (*16*). The reductive half-reaction, described above, consists of steps between LA binding through the irreversible $H^{\bullet}$ abstraction to generate $L^{\bullet}$. In contrast to the reductive half-reaction (*19*), the oxidative half-reaction is poorly understood. Following models for O_2 binding to myoglobin (Mb) (*22*), the chemical mechanism for O_2 interacting with SLO must include a kinetic step for O_2 motion through the protein to the deeply buried active site. A minimal chemical mechanism (Scheme 1) comprises diffusional encounter of SLO with O_2, migration of O_2 through the distal regions of SLO toward the vicinity of $L^{\bullet}$, reaction of O_2 to generate the peroxyl radical ($LOO^{\bullet}$), formation of protonated peroxide (LOOH) and oxidized enzyme (Fe^{3+}−OH), and release of product. $k_{cat}/K_M(O_2)$ is the second-order rate constant characterizing the steps from diffusional encounter with O_2 up to the first irreversible step, and mechanistic probes of this parameter can provide insight into the effect of protein on reactivity.

† This work was supported by a National Institutes of Health grant (GM 25765) to J.P.K. and a National Institutes of Health postdoctoral fellowship (F32-GM19843) to M.J.K.

* To whom correspondence should be addressed. Tel: 510-642-2668. Fax: 510-643-6232. E-mail: klinman@socrates.berkeley.edu.

‡ Current address: Department of Chemistry, University of Massachusetts, Amherst, MA 01003.

[1] Abbreviations: LA, linoleic acid [9,12-(*Z*,*Z*)-octadecadienoic acid]; $L^{\bullet}$, linoleyl radical; 13-(*S*)-HPOD, 13-(*S*)-hydroperoxy-9,11-(*Z*,*E*)-octadecadienoic acid; SLO, soybean lipoxygenase-1; Mb, myoglobin; $LOO^{\bullet}$, peroxylinoleyl radical; RP-HPLC, reversed-phase HPLC; $^{18}k_{cat}/K_M$, oxygen-18 kinetic isotope effect on k_{cat}/K_M; KIE, kinetic isotope effect; SIE, solvent isotope effect.

10.1021/bi0300884 CCC: $25.00
Published on Web 09/10/2003

Scheme 1: Oxidative Half-Reaction of Soybean Lipoxygenase[a]

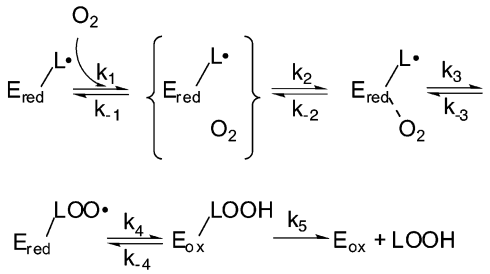

[a] E_{red} and E_{ox} denote the $Fe^{2+}-OH_2$ and the $Fe^{3+}-OH$ forms of SLO, respectively. L• denotes the linoleyl radical, LOO• denotes the peroxy−linoleyl radical, and LOOH is the product 13-(*S*)-HPOD.

Scheme 2: Stereochemistry of O_2 Insertion Relative to H• Abstraction from Substrate Catalyzed by Soybean Lipoxygenase[a]

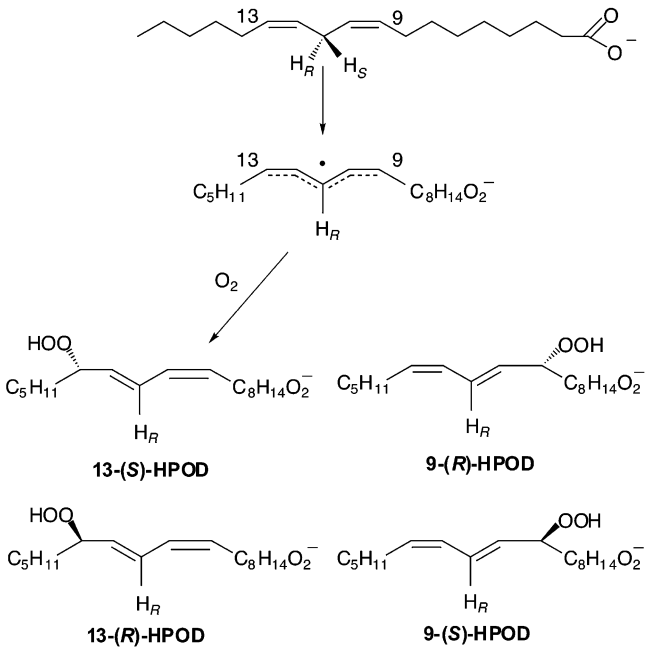

[a] Both 13-(*S*)-HPOD and 9-(*R*)-HPOD result from antarafacial O_2 insertion, whereas 13-(*R*)-HPOD and 9-(*S*)-HPOD result from suprafacial O_2 insertion.

SLO produces 13-(*S*)-HPOD with very high specificity (*1*), despite the possibility of radical delocalization over the C-9−C-13 pentadienylic moiety of L• (Scheme 2). Similar reactions between linoleyl radicals and O_2 in solution lead to equal distributions of 9-(*R*/*S*)-HPOD and 13-(*R*/*S*)-HPOD. This has generated much controversy over the means by which the biradical $\{^3O_2 + {}^2L^\bullet\}$ reaction can proceed with such high stereo- and regiospecificity on the enzyme. One proposal involves the direct involvement of Fe, proceeding through a peroxy−ferric intermediate $[L-O-O-Fe]^{2+}$ called "purple lipoxygenase", which imparts stereochemical control by virtue of the chemical influence of Fe (*23*). This proposal is supported by the spectroscopic isolation of $[L-O-O-Fe]^{2+}$ (*21*) and by a recent protein crystal structure of this intermediate (*24*). However, detection of the purple complex requires very high concentrations of [13-(*S*)-HPOD], suggesting that purple lipoxygenase lies off the catalytic pathway. A second proposal invokes protein structural elements that direct O_2 stereochemistry by virtue of proximal steric effects (*5*, *15*). This proposal is supported by the observation that O_2 insertion is antarafacial to the H• atom abstraction (*1*), implying that the Fe cofactor cannot be in the correct position for both C−H cleavage and catalytically productive purple lipoxygenase formation.

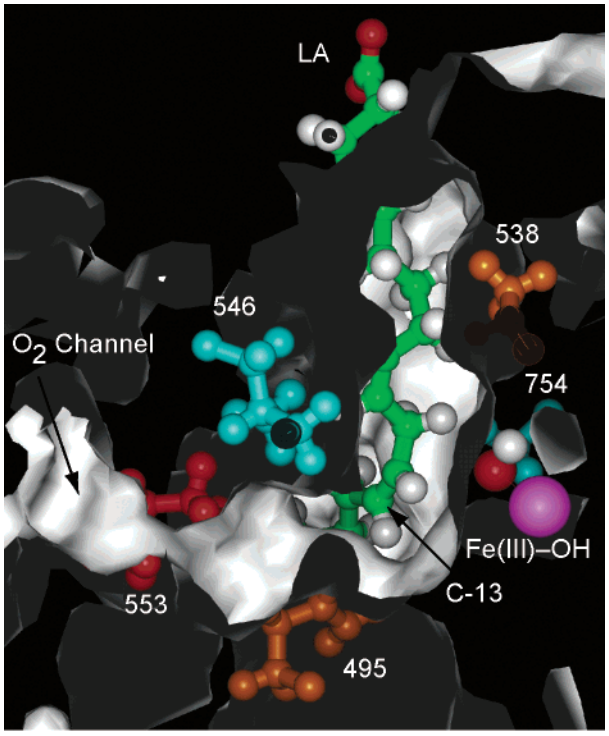

FIGURE 1: Substrate cavity and proposed O_2 access channel of SLO (from ref *34*). The substrate LA (C, green; H, white; O, red) has been modeled to bind with C-1 toward the top of the figure and C-9−C-13 positioned between Ile^{538} and Gln^{495} (orange). The proposed O_2 channel, above Ile^{553} (red), intersects the substrate cavity close to the C-13 position of LA. Leu^{546} and Leu^{754} (blue) constrict C-11 of LA. $Fe^{3+}-OH$ is presented as CPK spheres (Fe, magenta; O, red; H, white).

This laboratory has recently developed a suite of probes for O_2 chemistry that allows the identification of rate-limiting steps on $k_{cat}/K_M(O_2)$ (*25*). A combination of heavy atom isotope effects (^{18}O vs ^{16}O), solvent isotope effects (H_2O vs D_2O), and solvent viscosity effects has been used successfully to characterize O_2 activation chemistry in several enzymes (*26*−*33*). These steady-state probes can differentiate rate-limiting steps, such as diffusion or protonation, thereby lending support to mechanistic proposals.

The current report discusses O_2 chemistry during normal turnover of SLO, using a combination of kinetic probes of WT SLO and an active site mutant. A previous communication of product distributions in several active site mutants (*34*) was consistent with proximal protein effects (bulk of residues) determining the stereochemistry of product. A model for LA bound in cavity IIa (*7*) of SLO was presented (*34*) that illustrates the relative orientation of Fe, LA, and a side channel intersecting cavity IIa (Figure 1). The data presented herein appear to rule out diffusion, protonation, and outer-sphere electron transfer to O_2 as rate-limiting for $k_{cat}/K_M(O_2)$, indicating either a rate-limiting radical combination of O_2 with L• or a subsequent slow conformational change. It is observed that $Ile^{553} \rightarrow$ Phe decreases $k_{cat}/K_M(O_2)$ by a factor of 20, yet retains the same rate-limiting step as WT SLO. It is therefore argued that O_2 enters the enzyme via a side channel near Ile^{553}, followed by a rate-limiting

combination of $^3O_2$ with $^2L^\bullet$ in which proximal residues can impede the rate of reaction. These results support the growing view that enzymes can control O_2 reactivity through the use of appropriately configured amino acid side chains (*35*, *36*).

MATERIALS AND METHODS

Enzyme Preparation, Mutagenesis, and Reagents. Enzymes were expressed and purified as previously described (*10*, *34*, *37*). Buffers and other reagents were of ACS reagent grade or better and were used as received. Linoleic acid (99+% purity) purchased from Sigma was purified by RP-HPLC and stored as a 20 mM stock in methanol at −80 °C. This stock was diluted into the appropriate buffer to a final concentration of 1 mM for daily use. 13-(*S*)-HPOD was prepared by a previously reported method (*38*) and stored as a 10 mM stock in methanol at −80 °C. Perdeuterated LA (D_{31}-LA, 98% isotopic purity) was purchased from Cambridge Isotope Labs. Reaction with a small amount of SLO removed the minor protiated contamination and eliminated the burst phases commonly observed with samples of D_{31}-LA. SLO-scrubbed D_{31}-LA was then purified, stored, and diluted as per LA. 11,11-[$^2H_2$]-LA was a gift from Dr. Matt Meyer (University of California, Berkeley) and had been prepared by a method similar to that previously published (*37*).

Kinetic Determinations. All kinetic measurements were obtained by monitoring the consumption of O_2 with a Clark-type electrode. Reactions were stirred and thermostated at either 20 or 21 °C. LA (80 μM) was used in each kinetic run unless otherwise noted, and reactions were 1 mL in volume. The buffer (0.1 M borate, pH 9.00, unless otherwise noted) and substrate were allowed to equilibrate for ca. 5 min under a controlled O_2/N_2 atmosphere, and the reactions were initiated by addition of ca. 4 μL of concentrated enzyme via a gastight syringe. The concentration of O_2 in CHES and Tris buffers was calibrated by use of the protocatechuate dioxygenase/protocatechuate reaction, in which a defined amount of O_2 is consumed (*39*); however, borate inhibited this reaction. For reaction in borate, [O_2] was obtained from standard reference tables for pure H_2O (*40*).

Rates were linear for several minutes at elevated [O_2], although extensive lag phases were observed at reduced [O_2]. Thus, initial rates were recorded as the maximal, linear phase observed (≥10% of limiting reagent consumed), and the corresponding O_2 concentration was determined at the beginning of the linear phase. Initial rates were fitted by nonlinear least squares (*41*) to the Michaelis−Menten equation (*42*) (eq 1), where v_0 is the initial rate, $[E]_T$ is the total enzyme concentration, k_{cat} is the maximal velocity, and K_M is the Michaelis constant for O_2. Standard errors were propagated from these fits.

$$\frac{v_0}{[E]_T} = \frac{(k_{cat}/K_M)[O_2]}{1 + [O_2]/K_M} \quad (1)$$

The reductive half-reaction was monitored under conditions of nearly saturating [O_2] with the Clark-type electrode in 0.1 M borate, pH 9.00. WT SLO was analyzed under an ambient atmosphere ([O_2] = 288 μM), while $Ile^{553} \rightarrow Phe$ was analyzed under an atmosphere of pure O_2 ([O_2] ≈ 1300 μM). Initial rate data were collected by varying [LA] and fitted by nonlinear least squares to a version of eq 1 where [O_2] is replaced by [LA].

Effect of HPOD on $k_{cat}/K_M(O_2)$. The effect of 13-(*S*)-HPOD on $k_{cat}/K_M(O_2)$ was determined by measuring $k_{cat}/K_M(O_2)$ at variable [HPOD]. The concentration of 13-(*S*)-HPOD was determined as the sum of added 13-(*S*)-HPOD (0, 10, 20, or 40 μM) and the concentration of O_2 consumed during the lag phase. The observed $k_{cat}/K_M(O_2)$ data were fitted by nonlinear least squares (eq 2); K_A is the affinity constant for 13-(*S*)-HPOD, which is represented by [P]. This equation is derived in the Appendix.

$$\left(\frac{k_{cat}}{K_M(O_2)}\right)_{obs} = \frac{[k_{cat}/K_M(O_2)]_{max}}{K_A/[P] + 1} \quad (2)$$

pH Dependence and Solvent Isotope Effect on k_{cat}/K_M. Buffers were prepared with either 0.2 M borate (pH 8.5−10.0) or 0.2 M Tris (pH 7.5−8.5), the pH was adjusted with NaOH, and the ionic strength was adjusted to 0.2 M by addition of NaCl. D_2O-containing buffers were prepared by use of 99.9% D_2O in the place of H_2O, and the pD was adjusted with NaOD, where 0.4 was added to the reading of the pH meter ($pD = pH_{read} + 0.4$).

Solvent Viscosity Effect. These experiments were carried out in 0.1 M CHES buffer, pH 9.0, with varying amounts of glucose added as viscosogen. The relative viscosity was determined by use of an Ostwald viscometer and referenced to H_2O at 20 °C. [O_2] was determined in the presence of glucose, as discussed above.

Oxygen Isotope Effects. The ^{18}O kinetic isotope effect on $k_{cat}/K_M(O_2)$ [$^{18}k_{cat}/K_M(O_2)$] was determined by isotope-ratio mass spectrometry, using methods previously described (*29*, *32*, *43*). Borate buffer (0.1 M, pH 9.00) was saturated with O_2 (ca. 1 mM), and then LA was added to a final concentration of ca. 1 mM. The buffer was allowed to cool to 20 °C in a closed system before a blank was collected. Reaction was initiated by addition of enzyme via a gastight syringe, with subsequent time points analyzed.

RESULTS

Mechanistic Probes of $k_{cat}/K_M(O_2)$ in WT SLO. (A) Effect of HPOD on $k_{cat}/K_M(O_2)$. Addition of 13-(*S*)-HPOD altered the observed $k_{cat}/K_M(O_2)$ in a saturable manner, with increasing 13-(*S*)-HPOD leading to an increase in the observed $k_{cat}/K_M(O_2)$ (Figure 2). For WT SLO at 20 °C, fitting the observed $k_{cat}/K_M(O_2)$ vs [HPOD] curves to eq 2 resulted in parameters of $[k_{cat}/K_M(O_2)]_{max} = 21\ (\pm 1)\ \mu M^{-1}\ s^{-1}$ and $K_A = 6.2\ (\pm 1.2)\ \mu M$, indicating that 13-(*S*)-HPOD alters the distribution of enzyme between active ($Fe^{3+}-OH$) and inactive ($Fe^{2+}-OH_2$) pools under low [O_2] conditions. Thus, a maximal $k_{cat}/K_M(O_2)$ requires a high [HPOD]. In these experiments, 40 μM HPOD was sufficient to "saturate" $k_{cat}/K_M(O_2)$, and this concentration of added HPOD was used in several of the mechanistic probes (e.g., SIE, viscosity effect, pH effect).

(B) pH Dependence and Solvent Isotope Effect (SIE) on $k_{cat}/K_M(O_2)$. To measure the pK_a of enzyme-bound species (e.g., $Fe^{2+}-OH_2$) controlling $k_{cat}/K_M(O_2)$, this parameter was determined as a function of pH and plotted on a log scale (Figure 3). A single titratable proton would lead to a slope of ±1 in this log scale plot. Despite the scatter in the

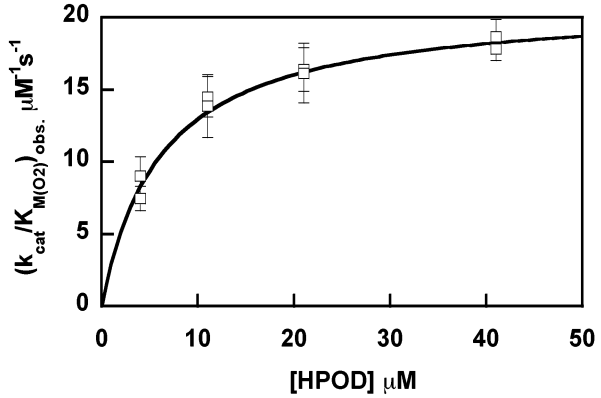

FIGURE 2: Effect of 13-(*S*)-HPOD on $k_{cat}/K_M(O_2)$ of soybean lipoxygenase (0.1 M borate, pH 9.0, 20 °C). The open squares are the observed $k_{cat}/K_M(O_2)$, with standard errors indicated. The solid line is the fit to eq 2, with the parameters $[k_{cat}/K_M(O_2)]_{max} = 21.0$ ($\pm$1) μM^{-1} s^{-1} and $K_A = 6.2$ ($\pm$1.2) μM. See text for details.

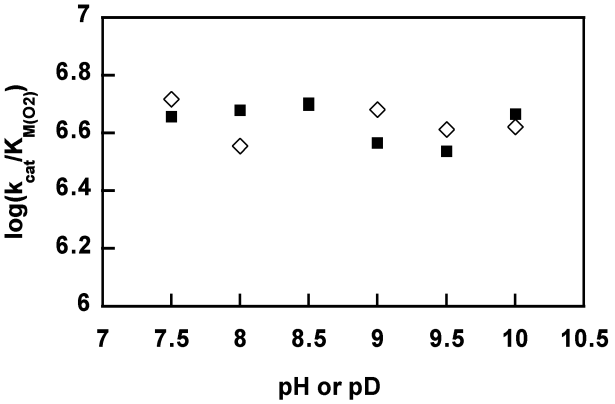

FIGURE 3: Effect of pH on $k_{cat}/K_M(O_2)$ in buffers containing H_2O (solid points) or D_2O (open points) at 21 °C. The reported pD in D_2O is obtained by adding 0.4 to the reading on the pH meter. $k_{cat}/K_M(O_2)$ is 4.28 ($\pm$0.2) μM^{-1} s^{-1} in H_2O, and the SIE is 1.06 ($\pm$0.08).

measured values, it is apparent that $k_{cat}/K_M(O_2)$ is essentially constant, and there is no titratable proton over the pH 7.5−10.0 range. Thus, the kinetic pK_a of $Fe^{2+}-OH_2$ is greater than 10.5. The kinetic data were averaged, resulting in a $k_{cat}/K_M(O_2) = 4.28$ ($\pm$0.2) μM^{-1} s^{-1} in H_2O.

The solvent isotope effect was measured over the same pH range by using buffers prepared with D_2O. In these experiments, one of the protons on the $Fe^{2+}-OH_2$ intermediate was expected to be ^1H, as it is derived from the nonexchanging *pro-S* hydrogen of C-11 on LA, while the second proton will be derived from solvent as either ^1H or ^2H. The data in D_2O are plotted (Figure 3) and averaged as for the H_2O data set. The resultant $k_{cat}/K_M(O_2)$ in D_2O-containing buffers is 4.04 ($\pm$0.22) μM^{-1} s^{-1}, leading to a solvent isotope effect of 1.06 ($\pm$0.08) under these conditions. The SIE was also determined with 40 μM HPOD added to 0.1 M borate buffer at $pH_{read} = 9.00$. Under these conditions, the SIE on $k_{cat}/K_M(O_2)$ was found to be 1.0 ($\pm$0.2).

The solvent isotope effect was also measured in 0.1 M borate, pL = 9.0, 21 °C, using [$^2H_{31}$]-LA. In this case a ^2H is derived from LA, while the solvent contributes either ^1H or ^2H. This provided a control in which both protons on $Fe^{2+}-OH_2$ are deuterated. Data below 7 μM O_2 could not be obtained, leading to only a rough estimate of $K_M(O_2)$ ($K_M \leq 2$ μM in both H_2O and D_2O). For this reason, only a lower limit for $k_{cat}/K_M(O_2)$ could be estimated [$k_{cat}/K_M(O_2) \geq 1.4$ μM^{-1} s^{-1} in H_2O; $k_{cat}/K_M(O_2) \geq 2.2$ μM^{-1} s^{-1} in D_2O], precluding a reliable value for the SIE under conditions of $Fe^{2+}-O(^2H)_2$.

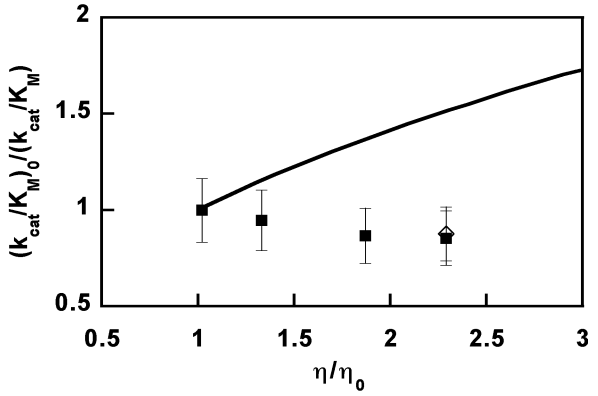

FIGURE 4: Effect of solvent viscosity on $k_{cat}/K_M(O_2)$ (0.1 M CHES, pH 9.0, 21 °C, glucose viscosogen). Data were collected both without added 13-(*S*)-HPOD (solid squares) and with 40 mM added 13-(*S*)-HPOD (open diamond at $\eta/\eta_0 = 2.26$). The line is the theoretical viscosity dependence of O_2 diffusion, $1/k_{rel} = (\eta_{rel})^{1/2}$, which has been reported previously when the substrate is O_2 (*44*).

(C) Solvent Viscosity Effect on $k_{cat}/K_M(O_2)$. Increased solvent viscosity was used to probe for rate-limitation from diffusional processes on $k_{cat}/K_M(O_2)$. The data were collected in 0.1 M CHES, pH 9.00, with glucose as the viscosogen, and have been summarized in a normalized format ($(K_M(O_2)/k_{cat})_{rel}$ vs η_{rel}) (Figure 4). The viscosity dependence of a diffusional step involving molecular O_2 and an enzyme has been described as $k_0/k = 1/k_{rel} \propto (\eta_{rel})^{1/2}$, where η_{rel} is the relative viscosity and k_0 is the rate in the absence of added viscosogen (*44*, *45*).

It is clear from Figure 4 that $[K_M(O_2)/k_{cat}]_{rel}$ is slightly decreased upon addition of glucose, rather than being increased as for a simple, diffusion-limited process. The same data set showed that k_{cat} was independent of viscosity. WT SLO is nearly saturated with O_2 under ambient conditions [$K_M(O_2) = 31$ μM] without added 13-(*S*)-HPOD, and therefore this result is a good estimate of the true k_{cat}. Data collected with 40 μM added HPOD showed a similar inverse viscosity effect [$[K_M(O_2)/k_{cat}]_{rel} = 0.88 \pm 0.14$] and inverse that the viscosity dependence of $[K_M(O_2)/k_{cat}]_{rel}$ was not altered by the partitioning of enzyme into an inactive pool.

(D) Reductive Half-Reaction of WT SLO. The reaction of WT SLO with LA was measured to obtain kinetic parameters for the reductive half-reaction under the conditions of the O_2 study. Under an ambient atmosphere, k_{cat} was observed to be 230 ($\pm$15) s^{-1}, and K_M(LA) = 18 ($\pm$3) μM, for a k_{cat}/K_M(LA) = 12.5 ($\pm$1.2) μM^{-1} s^{-1} (Table 1). WT SLO is nearly saturated with O_2 under ambient conditions [$K_M(O_2) = 31$ μM, without added 13-(*S*)-HPOD], and therefore this result is a good estimate of the true K_M(LA).

Mechanistic Probes of $k_{cat}/K_M(O_2)$ for $Ile^{553} \rightarrow Phe$. It was shown in a previous communication (*34*) that the $Ile^{553} \rightarrow$ Phe mutant leads to a reduced rate of oxygenation, without compromising the stereoselectivity of O_2 insertion in the SLO reaction. In addition, its principle kinetic effect is on the steps that determine $k_{cat}/K_M(O_2)$, with a minor reduction in k_{cat}. Kinetic probes of O_2 reactivity were, thus, applied to

Table 1: Comparison of Kinetic Parameters for WT SLO and $Ile^{553} \rightarrow$ Phe, 0.1 M Borate, pH 9.00, 20 °C

	WT SLO	$Ile^{553} \rightarrow$ Phe
k_{cat} (s^{-1})	230 (±15)	102 (±8)
$K_{M(LA)}$ (μM)	18 (±3)	19 (±4)
$k_{cat}/K_M(O_2)$ (μM^{-1} s^{-1})[a]	7.5 (±0.9)	0.72 (±0.3)
$k_{cat}/K_M(O_2)$ (μM^{-1} s^{-1})[b]	21 (±1)	0.96 (±0.08)
SIE	0.98 (±0.1)	1.06 (±0.08)
^{18}O KIE	1.0115 (±0.0013)[c]	1.0105 (±0.0008)

[a] Under conditions of no added 13-(*S*)-HPOD. [b] Extrapolated to saturating 13-(*S*)-HPOD. [c] See ref *29*.

$Ile^{553} \rightarrow$ Phe to identify rate-limiting steps on $k_{cat}/K_M(O_2)$ for comparison to WT SLO.

(A) Effect of HPOD on $k_{cat}/K_M(O_2)$ of $Ile^{553} \rightarrow$ Phe. Addition of 13-(*S*)-HPOD was determined to have a small effect on the observed $k_{cat}/K_M(O_2)$ for $Ile^{553} \rightarrow$ Phe while diminishing the lag phases significantly. Without added 13-(*S*)-HPOD, $k_{cat}/K_M(O_2) = 0.72$ (±0.03) μM^{-1} s^{-1}, and extensive lag phases were observed. Upon addition of 40 μM 13-(*S*)-HPOD this rate constant increased slightly, $k_{cat}/K_M(O_2) = 0.84$ μM^{-1} s^{-1} (± 0.03), and the lag phase disappeared. Fitting the observed $k_{cat}/K_M(O_2)$ vs [HPOD] curves to eq 2 resulted in parameters of $[k_{cat}/K_M(O_2)]_{max} = 0.96$ (±0.08) μM^{-1} s^{-1} and $K_A = 6.5$ (±2.8) μM, indicating a K_A similar to that seen in WT SLO. The extensive lag phases observed with the slower $Ile^{553} \rightarrow$ Phe led to a high [HPOD] once the linear phase was reached, even when no 13-(*S*)-HPOD was intentionally added; thus the observed $k_{cat}/K_M(O_2)$ always reflects conditions under which enzyme is dominantly in the active pool [$[k_{cat}/K_M(O_2)]_{max}$ is 0.96 μM^{-1} s^{-1} at saturation vs 0.84 μM^{-1} s^{-1} in the absence of HPOD].

(B) pH Dependence and Solvent Isotope Effect on $k_{cat}/K_M(O_2)$ of $Ile^{553} \rightarrow$ Phe. No effect of pH was observed between pH 8.00 and pH 10.00 in buffers made from either 0.1 M Tris (pH 8.00) or 0.1 M borate (pH 9.00, 10.00) in H_2O. Thus, $Ile^{553} \rightarrow$ Phe did not measurably perturb the pK_a of the active site proton donor. The SIE on $k_{cat}/K_M(O_2)$, measured at a single pH, was 0.98 (±0.1) (0.1 M borate, pH 9.0); this is within error of unity, as seen in WT SLO.

The solvent isotope effect was also measured in 0.1 M borate, pL = 9.0, 21 °C, using 11,11-[$^2H_2$]-LA. As described for WT SLO, the hydrogen derived from LA in $Fe^{2+}-OH_2$ will be ^2H, while that from solvent is either ^1H or ^2H. This provided a control, in the event that the two protons of $Fe^{2+}-OH_2$ exchanged slowly. With deuterated substrate, the rate of reaction did not slow measurably at reduced [O_2], and consequently, $K_M(O_2)$ could only be estimated to be below 5 μM in both H_2O and D_2O. This leads to a lower limit for $k_{cat}/K_M(O_2)$ which could only be estimated (as ≥ 0.5 μM^{-1} s^{-1}) in both H_2O and D_2O.

(C) Solvent Viscosity Effect on $k_{cat}/K_M(O_2)$ of $Ile^{553} \rightarrow$ Phe. The solvent viscosity effect on $k_{cat}/K_M(O_2)$ was determined by comparing this rate constant with or without 30% glucose added to 0.1 M CHES, pH 9.00. The measured viscosity effect was $[K_M(O_2)/k_{cat}]_{rel} = 0.8$ (±0.2), a value that compared well to that observed in WT SLO. It was concluded that diffusional encounter between O_2 and enzyme was not rate-limiting. As with WT SLO, a potential origin of the inverse viscosity effect is a nonspecific structural perturbation of the protein in the presence of a high concentration of glucose.

(D) Oxygen Isotope Effects in $Ile^{553} \rightarrow$ Phe. The ^{18}O isotope effect on $k_{cat}/K_M(O_2)$ was measured for this mutant to probe for changes from WT SLO. The kinetic isotope effect on $k_{cat}/K_M(O_2)$, given by the relative rate of reaction for $^{16}O^{16}O$ vs $^{18}O^{16}O$, was determined to be $^{18}k_{cat}/K_M(O_2) = 1.0105$ (±0.0008). In comparison, the ^{18}O KIE for WT SLO was reported as $^{18}k_{cat}/K_M(O_2) = 1.0115$ (±0.0013) (*29*). The ^{18}O KIEs are essentially identical and indicate that the rate-limiting step for $k_{cat}/K_M(O_2)$ is unaltered in this mutant.

(E) Reductive Half-Reaction of $Ile^{553} \rightarrow$ Phe. The reaction of $Ile^{553} \rightarrow$ Phe with LA was measured as a frame of reference for the O_2 reaction. Under an atmosphere of pure O_2 ([O_2] ≈ 1300 μM) k_{cat} was observed to be 102 (±8) s^{-1}, and $K_M(LA) = 19$ (±4) μM, for a $k_{cat}/K_M(LA) = 5.4$ (±0.7) μM^{-1} s^{-1} (Table 1). $Ile^{553} \rightarrow$ Phe is nearly saturated with O_2 under these conditions [$K_M(O_2) = 142$ μM, without added 13-(*S*)-HPOD], such that this result gives a good estimate of the true k_{cat} and $K_M(LA)$.

DISCUSSION

Effect of 13-(S)-HPOD on Enzyme Partitioning into the Inactive Pool. Pronounced lag phases were observed at low O_2 tensions during these studies, in particular for the $Ile^{553} \rightarrow$ Phe mutant. It was also observed that $K_M(O_2)$ would increase if buffers were allowed to age in polypropylene tubes over 1 week, presumably due to leaching of plasticizers; storing buffers in glass containers eliminated this effect. It has been shown previously that the substrate radical ($L^\bullet$) dissociates from the enzyme in the steady state, leading to production of an inactive pool of Fe^{2+} enzyme and a lag phase (*46*). The only known oxidant for Fe^{2+} SLO is the product, 13-(*S*)-HPOD (*47*), which is essential for full enzymatic activity (*46*). The above observations are attributable to SLO preferentially partitioning into this inactive pool due to slow reoxidation of inactive Fe^{2+} enzyme. When productive turnover is very slow, such as under conditions of subsaturating [O_2], the pool of inactive Fe^{2+} form is increased due to a deficiency in 13-(*S*)-HPOD and a reduced rate of reoxidation. Additionally, anti-oxidants (such as plasticizers) likely scavenge 13-(*S*)-HPOD, providing an explanation for the observed increases in $K_M(O_2)$ after aging buffers in polypropylene. The pool of inactive enzyme can be eliminated by addition of ca. 40 μM 13-(*S*)-HPOD to the kinetic assays, leading to an increase in initial rates under low [O_2] conditions, which in turn leads to a decrease in the observed $K_M(O_2)$.

Referring to Scheme 3 (see Appendix), K_A is the ratio of the rate constant for $L^\bullet$ loss (k_4) to the rate constant for reactivation by HPOD (k_5). The similar K_A for both WT and $Ile^{553} \rightarrow$ Phe indicates that the rate of $L^\bullet$ loss and the rate of reactivation are likely to be unchanged upon mutation. K_A provides an estimate of the rate of $L^\bullet$ loss (k_4), if a reasonable value for k_5 is available. k_5 is a composite of the unimolecular rate of oxidation by HPOD (k_{ox}) divided by the affinity constant for HPOD (K_{eq}), which have previously been estimated as 150 s^{-1} and 20 μM, respectively (*48*). Thus, k_5 in Scheme 3 is approximately 7.5 μM^{-1} s^{-1}, leading to an estimated rate of $L^\bullet$ loss as $k_4 \approx 1$ s^{-1}.

This is significantly below a previous estimate of k_4, ca. 2.3×10^3 s^{-1} for SLO, from Schilstra et al. (*48*, *49*). We

note that Schilstra et al. relied upon kinetic data collected at relatively high [O_2], which likely did not adequately reproduce the manner in which EL$^\bullet$ partitions between formation of ELOO$^\bullet$ vs E + L$^\bullet$ (*48*). Recently, Berry et al. included kinetic and product analysis data under low [O_2] conditions to analyze the inactivation of SLO during abortive turnover, reporting that k_4 is roughly 10 times smaller than the rate of H$^\bullet$ abstraction [known to be ca. 300 s^{-1} (*20*, *48*)] (*49*, *50*). In the case of reticulocyte lipoxygenase under conditions of low O_2, a value of $k_4 = 16\ s^{-1}$ has been estimated (*51*). Our estimate of $k_4 \approx 1\ s^{-1}$ suggests that loss of L$^\bullet$ from SLO is significantly slower than previously reported.

The extensive lag phase observed for Ile^{553} → Phe could have indicated that partitioning of enzyme into the inactive pool is more pronounced due to an increase in the rate of loss of L$^\bullet$ (k_4). However, since K_A is unchanged, this would require that k_5 also be increased for Ile^{553} → Phe. A more likely explanation for the extensive lags is a decrease in the rate of O_2 reacting with EL$^\bullet$ (k_2). This is supported by the finding that $k_{cat}/K_M(O_2)$ is markedly reduced in this mutant.

Rate-Limiting Steps on $k_{cat}/K_M(O_2)$ for WT SLO and Ile^{553} → Phe. SLO follows an ordered mechanism that reduces to ping-pong kinetics, making $k_{cat}/K_M(O_2)$ independent of kinetic processes preceding the initial encounter between O_2 and the enzyme. Thus, measuring $k_{cat}/K_M(O_2)$ under various conditions reveals only those steps that contribute to rate limitation on the oxidative half-reaction. The minimal model (Scheme 1) comprises O_2 diffusional encounter, O_2 motion through distal regions of SLO, O_2 reacting with L$^\bullet$ from proximal regions of the protein, a net H$^\bullet$ transfer from $Fe^{2+}-OH_2$ to generate LOOH and $Fe^{3+}-OH$, and product release. Mechanistic probes of $k_{cat}/K_M(O_2)$ will be sensitive to only those steps between the diffusional encounter with O_2 and the first irreversible step.

The absence of a viscosity effect on $k_{cat}/K_M(O_2)$ in WT SLO and the Ile^{553} → Phe mutants excludes both the diffusional encounter with O_2 and the diffusion of product away from enzyme as the rate-limiting step on this rate constant. The slight increase in $k_{cat}/K_M(O_2)$ at elevated viscosity could be due to a nonspecific perturbing effect of glucose on protein structure or dynamics and is opposite to the trend expected for a diffusion-limited process. In other enzyme systems, similar observations of increased rate at elevated viscosity have been attributed to nonspecific effects (*52*, *53*). We note that SLO appears to be very sensitive to solvent additives, as there are several reports of spectroscopic changes in response to millimolar concentrations of alcohols or glycerol (*10*, *17*, *54*, *55*).

Whenever possible, it is desirable to control for nonspecific interactions due to solvent additives. In previous studies, slow substrates or slow mutants have been used as controls to normalize enzyme activity in the presence of viscosogenic agents (*52*, *53*). SLO is very particular for its substrates (both LA and O_2), making a slow substrate unavailable. However, it was possible to examine the effect of viscosity on $k_{cat}/K_M(O_2)$ in the slow mutant of SLO, Ile^{553} → Phe, showing an effect that is identical to WT SLO. Thus, in neither case is diffusion rate-limiting, indicating that O_2 establishes an equilibrium ($K_{diff} = k_1/k_{-1}$) between O_2(aqueous) and O_2(bound) prior to the rate-limiting step.

No titratable proton was observed in this study, indicating that the proton donor in HPOD formation (presumably $Fe^{2+}-OH_2$) is fully protonated over the pH 7.5−10.0 range. This places the kinetically determined pK_a for this group at greater than 10.5, in full agreement with spectroscopic measurements of WT SLO that estimated a pK_a > 11 for $Fe^{2+}-OH_2$ (*10*). The SIE on $k_{cat}/K_M(O_2)$ is unity in both WT SLO and Ile^{553} → Phe, ruling out a step involving proton transfer between the $Fe^{2+}-OH_2$ cofactor and LOO$^\bullet$ (e.g., k_4 of Scheme 1) as rate-limiting. Such a protonation step would be anticipated to lead to a SIE in excess of 2 (*56*) if it were fully rate-limiting on $k_{cat}/K_M(O_2)$. While the above data cannot rule out an SIE of up to ca. 1.1, this would suggest only partial rate limitation by protonation, implicating (an)other step(s) as dominantly rate-limiting on $k_{cat}/K_M(O_2)$.

One of the protons of the aquo ligand to $Fe^{2+}-OH_2$ is derived from solvent and the other from the *pro-S* hydrogen of C-11 from LA. The possibility that only the proton derived from LA is ultimately transferred to LOO$^\bullet$, thereby obscuring any effect of solvent on this process, was investigated by SIE measurements using [$^2H_{31}$]-LA and 11,11-[$^2H_2$]-LA as substrate with WT SLO and Ile^{553} → Phe, respectively. These SIE measurements are hindered by the extremely low $K_M(O_2)$ for both WT SLO and the mutant with deuterated LA, making it impossible to collect data below $K_M(O_2)$. While $k_{cat}/K_M(O_2)$ with deuterated substrate is, thus, imprecise for both WT SLO and the Ile^{553} → Phe mutant, there does not appear to be an appreciable SIE in either case. We conclude that there is no evidence for a step involving proton transfer as rate-limiting on $k_{cat}/K_M(O_2)$.

The remaining potential rate-limiting steps are diffusion of O_2 through the protein (k_2), the radical reaction between O_2 and L$^\bullet$ (k_3), and two steps that have not been drawn in Scheme 1. These latter are (i) a rate-limiting conformational change between any of the two species shown and (ii) a rate-limiting outer-sphere electron transfer from $Fe^{2+}-OH_2$. This electron transfer could either reduce O_2 to form $O_2^{\bullet-}$, which then recombines with L$^\bullet$, or reduce LOO$^\bullet$ to form LOO^-, which would then be protonated to make LOOH (this breaks k_4 into two steps).

The observation of an ^{18}O KIE ($k_{16}/k_{18} = 1.01$, Table 1) eliminates a number of these steps from further consideration. A conformational change that precedes a change in bond order to oxygen, such as a conformational change prior to formation of LOO$^\bullet$, or the diffusion of O_2 from a distal to proximal position in the protein is inconsistent with a non-unity ^{18}O KIE. The magnitude of the ^{18}O KIE argues against an outer-sphere electron-transfer mechanism, since rate-limiting formation of $O_2^{\bullet-}$ or LOO^- would be expected to yield values greater than 1.01. Although a rather small ^{18}O KIE has, in fact, been observed earlier in the copper amine oxidase reaction, this is likely due to some interaction between the active site Cu^{2+} and the incipient superoxide (*32*, *35*). As we discuss below, there is no compelling evidence for interaction of any oxygen species with the active site iron in lipoxygenase. A conformational change limiting the breakdown of LOO$^\bullet$ is unlikely, as this would lead to the loss of LOO$^\bullet$ during abortive turnover; all previous analyses of abortive turnover in SLO can be fully explained by loss of L$^\bullet$ (*46*, *49*). Additionally, the reduction of LOO$^\bullet$ by $Fe^{2+}-OH_2$ may be anticipated to be fast, by virtue of the close approach of LOO$^\bullet$ and $Fe^{2+}-OH_2$ within cavity IIa (*57*).

We are, therefore, left with two possibilities for the rate-limiting step: formation of a peroxyl radical (LOO•) or a conformational change that limits product release. Within the context of Scheme 1, the first possibility is fully consistent with the ^{18}O KIE if one considers an isotope-insensitive preequilibrium, $K_{eq} = K_{diff}K_{distal}$. The observed ^{18}O KIE would then result from a kinetic effect on k_3, such that $^{18}k_{cat}/K_M = {}^{18}k_3$; in fact, the observed ^{18}O KIE is precisely that predicted for the reaction of O_2 with a radical (*33*).

Given that k_3 is a biradical combination, it would be expected to exhibit a magnetic isotope effect in which $^{17}O^{16}O$ reacts faster than $^{16}O^{16}O$, due to the hyperfine interaction between the ^{17}O nucleus and the incipient radical pair $\{^3O_2 + {}^2L^\bullet\}$. Hyperfine interactions promote intersystem crossing (*58*), thereby increasing the probability of the radical pair having the doublet configuration necessary to form product. Although magnetic oxygen isotope effects have been examined and were not observed on $k_{cat}/K_M(O_2)$ for SLO (*29*), this is most likely due to a dominance of intersystem crossing effects by the Fe^{2+} cofactor which may be expected to overwhelm any magnetic effect due to hyperfine interactions with the oxygen nuclei. Both the narrowness of cavity IIa and the large spin of Fe^{2+} ($S_T = 2$) are likely to promote very effective dipolar spin relaxation with the nearby $\{^3O_2 + {}^2L^\bullet\}$ radical pair.

Although the data with WT SLO are consistent with the rate-limiting formation of LOO•, it is not possible to eliminate a rate-limiting conformational change prior to product release (cf. ref *29*). However, comparison of WT SLO to $Ile^{553} \rightarrow$ Phe provides further insight. Two key observations are that the ^{18}O KIE for $Ile^{553} \rightarrow$ Phe is identical to that for WT SLO while the $k_{cat}/K_M(O_2)$ is reduced by a factor of 20. This indicates a common rate-limiting step that is slowed by the presence of Phe at position 553. Both the structural model of bound LA, showing that the side chain from residue 553 lies near to C-13, and the antarafacial nature of O_2 insertion relative to H• abstraction from C-11 by the active site iron are consistent with a role for protein groups near residue 553. If O_2 attack from this region of the protein is rate-limiting, it becomes easy to understand why the added bulk due to the $Ile^{553} \rightarrow$ Phe mutation impedes the rate of O_2 combination with L•.

The alternative, a rate-limiting conformational change, would attribute the reduction in $k_{cat}/K_M(O_2)$ for $Ile^{553} \rightarrow$ Phe to altered binding interactions with the fatty acid. If a change in protein structure affects a conformational change that limits $k_{cat}/K_M(O_2)$, this would be expected to show up in K_M-(LA); this latter parameter reflects binding interactions between LA and the enzyme as C−H bond cleavage largely limits the first half-reaction (*19*). However, under conditions close to O_2 saturation, K_M(LA) for Ile → Phe was found to be unchanged from WT SLO (cf. Table 1), indicating that the binding of LA to the enzyme was not appreciably changed upon mutation. While mutation of Ile^{553} to Ala has been shown to alter the temperature dependence of the primary hydrogen isotope effect for LA oxidation, the rate of C−H activation for fully protiated LA is also unchanged at room temperature (*59*). These observations make it unlikely that the binding or dynamics of any subsequent intermediate, such as LOOH, is altered upon mutation.

The existing kinetic data indicate that the initial reaction of L• with O_2 from proximal regions of the protein limits $k_{cat}/K_M(O_2)$. Such a mechanism is consistent with both the kinetic probes and the observation of L• dissociation under abortive turnover (*49*). As noted above, this mechanism requires that dipolar interactions with Fe^{2+} accelerate intersystem crossing within the incipient $\{^3O_2 + {}^2L^\bullet\}$ radical pair, facilitating the reaction and removing any magnetic isotope effect due to oxygen nuclei. In previous studies of the rate-limiting step in O_2 activation in the flavin-containing glucose oxidase (*31*, *36*), the TPQ, copper-containing copper amine oxidases (*32*, *35*), and the pterin, iron-containing tyrosine hydroxylase (*28*), the initial electron transfer to molecular oxygen has been concluded to represent the highest barrier in the $k_{cat}/K_M(O_2)$ free energy profile. The present study comes to very similar conclusions with regard to lipoxygenase, i.e., rate limitation by the initial chemical step with O_2, which, in this case, involves combination of prebound $^3O_2$ with $^2L^\bullet$. These similar catalytic strategies across different enzyme classes suggest that minimizing the accumulation of oxygenated free radical intermediates during enzyme turnover is evolutionarily favored.

Effect of Mutations on Oxygenation Stereochemistry. In a prior communication, we presented an energy-minimized model of LA bound into cavity IIa to illustrate the role of proximal protein structural effects on the C-8−C-14 region of substrate (*34*). Six residues (Gln^{495}, Trp^{500}, Ile^{538}, Leu^{546}, Ile^{553}, and Leu^{754}) provided the bulk of surface area in this region of cavity IIa. Leu^{546} and Leu^{754} formed a narrow pinch at C-11, thereby dividing bound substrate into an upstream half, defined by C-1−C-10, and a downstream half, defined by C-12−C-18. A side channel intersecting cavity IIa between Gln^{495} and Ile^{553} was seen to provide access of solvent and solutes to the downstream half of LA in a region antarafacial to the iron (reproduced in Figure 1). It was noted that access of O_2 to L• from this channel would produce the correct stereochemistry and regiochemistry to form 13-(*S*)-HPOD, the dominant product for WT SLO. Kinetic and product analysis on WT SLO and a series of mutants supported the view that O_2 did, indeed, enter SLO via this side channel undergoing addition to C-13 of substrate in the vicinity of residue 553 (*34*). These previous results are discussed below in relation to the present analysis of rate-limiting steps.

With regard to the magnitude of $k_{cat}/K_M(O_2)$, $Ile^{553} \rightarrow$ Phe was the only mutant with a principle kinetic effect, attributed to an impact of the increased bulk of this residue on O_2 reactivity. By contrast, Leu^{546} and Leu^{754} had only a minor effect on $k_{cat}/K_M(O_2)$ while reducing k_{cat} 100−1000-fold (*34*). Loss of bulk at either Leu^{546} or Leu^{754} has been concluded to result in nonoptimal positioning of LA for H• abstraction (*59*).

Product distributions were analyzed by chiral-phase HPLC analysis, and it was found that WT SLO and most of the mutants produced a single product as the dominant stereoisomer [>93% 13-(*S*)-HPOD]. In contrast, the $Leu^{546} \rightarrow$ Ala mutant produced 9-(*R*)-HPOD (≅10%) in addition to 13-(*S*)-HPOD, whereas the $Leu^{754} \rightarrow$ Ala mutant produced all four HPOD stereoisomers at appreciable levels (≥10%), as well as minor products that were attributed to all-trans HPODs (*34*). These results demonstrated that the two residues closest to the Fe cofactor, Leu^{546} and Leu^{754}, impart a significant proximal protein effect in determining the stereo- and regiochemistry of oxygenation. Due to the pinch

formed by Leu[546] and Leu[754] in WT SLO, solutes cannot access portions of L$^\bullet$ that lay upstream from C-11 (e.g., C-9). This prevents O_2 access to any radical character that may develop at C-9, making C-13 the only viable point of O_2 insertion. Both Leu[546] → Ala and Leu[754] → Ala reduce the barrier provided by this pinch, permitting O_2 to react at C-9. It is notable that the two HPOD products from Leu[546] → Ala have 13-(*S*) and 9-(*R*) stereochemistry, entirely consistent with O_2 attack on L$^\bullet$ from the face opposite that of H$^\bullet$ abstraction, though with a somewhat decreased selection between the readily accessed C-13 and the less accessible C-9. Leu[754] → Ala shows a wider product distribution, while remaining biased in favor of HPODs with 13-(*S*) and 9-(*R*) stereochemistry. Apparently, Leu[754] → Ala creates a much more relaxed substrate-binding mode than any other mutant, as shown by the 1000-fold reduction in k_{cat} and by the appearance of low levels of what appeared to be the all-trans HPODs (*34*).

The product distributions also provided some insight into the structure of the linoleyl radical, L$^\bullet$, indicating that radical character likely develops at both C-9 and C-13 (*34*). The seven carbons that make up the pentadienyl moiety of LA (C-8−C-14) lay in a sharp bend of cavity IIa bordered by Gln[495] and Ile[538]. These residues are too closely spaced to allow the pentadienyl group to become planar, as previously noted (*7*). The most straightforward way for O_2 to react with L$^\bullet$ is at a site of unpaired electron density, which in view of the steric congestion in cavity IIa may be a Δ^9-[11,12,13] ene-allyl radical, causing O_2 to react at C-13. However, the only experimental work to address the delocalization pattern of the L$^\bullet$ in SLO determined the linoleyl radical on SLO to be a [9,10,11]-Δ^{12} allyl-ene radical, with unpaired spin density at C-9, leading to a unique mechanistic proposal (*23*).

With LA modeled in the "head-out" orientation, Gln[495] and Ile[538] were found to interact with C-14 and C-8, respectively (*34*). By relieving steric congestion, mutants at these positions were expected to alter the relative stability of the three likely radicals: [9,10,11]-Δ^{12} and Δ^9-[11,12,-13] ene-allyl radicals and the [9,10,11,12,13] pentadienyl radical. However, Gln[495] → Ala and Ile[538] → Ala changed neither $k_{cat}/K_M(O_2)$ nor the stereochemical product distribution, implying that the reaction with O_2 was not altered in any way by reducing the bulk of residues at these positions. It has been concluded that either an ene-allyl radical does not form during turnover or else the [9,10,11]-Δ^{12} radical rapidly interconverts with the Δ^9-[11,12,13] radical, thereby leading to sufficient unpaired spin density at both C-9 and C-13 for radical reaction with O_2 (*34*).

We conclude that product distribution in the WT SLO and its mutants is under kinetic control, with O_2 preferentially reacting in a rate-limiting step, on the *pro-S* face of C-13. If O_2 simply diffused through the protein to L$^\bullet$, a wide product distribution would be expected for this biradical reaction in the absence of protein proximal effects. Thermodynamic control over HPOD regio- and stereochemistry would imply that an equilibrium is established at the stage of either LOO$^\bullet$ or LOOH, implicating a rate-limiting step on $k_{cat}/K_M(O_2)$ after LOO$^\bullet$ formation. However, the extensive mechanistic arguments outlined above argue against this possibility.

Mechanism of the O_2 Half-Reaction. The proposal of an O_2 channel in SLO rests on both kinetic and product analyses of site-directed mutants and a structural model derived from the crystal structure of SLO. These results lead to the following mechanism of O_2 reaction with SLO: O_2 reversibly diffuses to the surface of SLO; O_2 then moves through distal regions of the protein (the side channel to cavity Ila); O_2 reacts with L$^\bullet$ from a proximal region of SLO to form LOO$^\bullet$, this being the probable rate-limiting step; net H$^\bullet$ ($H^+ + e^-$) transfer from $Fe^{2+}-OH_2$ forms LOOH and $Fe^{3+}-OH$; and, finally, product is released to regenerate the resting enzyme.

A kinetic model for the oxidative half-reaction of SLO that involves a rate-limiting reaction of O_2 with L$^\bullet$ near Ile[553] provides a unified view of the available kinetic and product distribution data, while accounting for the observation that $k_{cat}/K_M(O_2)$ is reduced by a factor of 20 in the Ile[553] → Phe mutant without altering the nature of the rate-limiting steps (Table 1). Additionally, K_M(LA), which approximates K_D for substrate (*59*), appears to be unchanged for Ile[553] → Phe (Table 1), supporting the view that the mode of LA binding is similar to WT SLO, and implies that this mutant simply impedes the rate of O_2 access to L$^\bullet$. The side channel, which passes residue 553 (Figure 1), is an obvious route for solutes to access L$^\bullet$. Only those mutants near C-11 of the substrate, Leu[546] → Ala and Leu[754] → Ala, lead to reduced stereochemical control over O_2 insertion (*34*). It is hard to rationalize how mutations at the middle of the pentadienyl moiety can alter product distribution, unless they relax a kinetic barrier that normally prevents O_2 from accessing C-9 of L$^\bullet$. These amino acid side chains appear to form a barrier between the upstream portion of LA (C1−C11) and the side channel.

Our proposal that O_2 enters through a channel to attack C-13 of the linoleyl radical is entirely consistent with the [+2] registry and antarafacial nature of O_2 insertion in arachidonic acid oxygenations by mammalian LOs (*5*). Mammalian LOs catalyze stereospecific O_2 insertion into C-5, C-12, or C-15 of arachidonic acid following H$^\bullet$ abstraction from C-7, C-10, or C-12, respectively (*5*). This has led to two models for this specificity, the "orientation" model and the "space-filling" model. In the orientation model, it is proposed that regiospecificity of O_2 insertion is determined by the direction of substrate binding; "head-in" leads to 5-peroxy products, while "head-out" leads to 12- and 15-peroxy products. The space-filling model implies that it is the available volume within the LA-binding pocket that determines how deeply the methyl tail can go, thereby determining the registry between H$^\bullet$ abstraction and O_2 insertion (*15*). While the latter model has difficulty with the stereospecificity of 5-LO, we note that if 12- vs 15-LO specificity is determined by the volume of the substrate channel, and if 5-LO specificity results from head-in binding, this could account for both the stereochemistry and regiochemistry of mammalian LOs (*60*, *61*).

The experiments described herein do not directly address the relevance of a putative $[Fe-OOL]^{2+}$ intermediate, the "purple" lipoxygenase, to the catalytic cycle. They do, however, indicate that such an intermediate is not necessary and is unlikely to be catalytically relevant. The fact that active site mutations affect product distribution at all implies that the stereospecificity of O_2 insertion into L$^\bullet$ does not require a chemical interaction with the active site iron. Finally, k_{cat} is fully rate-limited by the H$^\bullet$ abstraction ($k_{H^\bullet} = k_{cat} \approx 230$ s^{-1}), and thus, decay of all subsequent intermediates must be much faster than this rate; yet purple LO decays relatively

Scheme 3

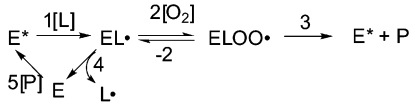

slowly at low temperatures (*21*). On this kinetic basis, purple SLO appears to be a poor candidate for a reactive intermediate. It seems far more likely that purple SLO is involved in the reactivation of the inactive pool of SLO that results from loss of L$^\bullet$ from the enzyme (Scheme 3).

This work implies some unusual features regarding O_2 chemistry. For one, the idea of O_2 entering via a specific protein channel is not widely accepted; however, we note that O_2 binding in myoglobin (Mb) has been shown to involve several hydrophobic sites independent of the heme iron, some of which serve as low-affinity binding sites (*62*−*65*). That body of work is extensive, including structural characterization of a Xe binding site (*66*), and it appears irrefutable that discrete hydrophobic pockets are involved in gas interactions with Mb. Rather than invoking such a discrete binding site in SLO, we merely suggest that there is a channel serving as a diffuse O_2 reservoir. Although it has been observed that SLO has a high affinity for Xe (*67*), it is not necessary that this channel have a high affinity for O_2. Rather, it is proposed to provide a way station between O_2 dissolved in bulk water and O_2 which becomes chemically bonded as LOO$^\bullet$. This separates the $O_2 + L^\bullet \rightarrow LOO^\bullet$ reaction into three kinetic steps: diffusion from bulk water (k_1), motions through distal regions of SLO (k_2), and finally attack on L$^\bullet$ from proximal regions of SLO (k_3). Such a three-step model is analogous to proposals for ligand binding to Mb (*22*).

ACKNOWLEDGMENT

We thank Dr. Julia Thrower (University of California, Berkeley) for help with deriving kinetic expressions and Dr. Matthew Meyer (University of California, Berkeley) for providing 11,11-[$^2H_2$]-LA.

APPENDIX

Kinetic Treatment of Lipoxygenase Activation by HPOD. The kinetic scheme for the reactivation of SLO by HPOD (Scheme 3) is based on earlier work by Schilstra et al. (*46*, *48*). E* represents the active form of SLO (Fe^{3+}−OH), E represents the Fe^{2+}−OH_2 form of SLO, L is linoleic acid, P is 13-(*S*)-HPOD, and L$^\bullet$ is the intermediate linoleyl radical. This scheme assumes that several steps are irreversible and incorporates several composite rate constants for the sake of clarity.

The assumption of an irreversible reaction with LA ($k_{-1} = 0$) is only justified if we restrict our analysis to saturating [LA]. k_5 is the composite second-order rate constant for reactivation of enzyme, representing the reaction of HPOD with the Fe^{2+} form of SLO, and includes both binding and reaction of HPOD. The release of L$^\bullet$, k_4, will be kinetically irreversible under initial conditions of low [L$^\bullet$]. This scheme ignores potential product inhibition on k_1 and neglects the potential for micromolar levels of product to make k_3 reversible.

Using the King−Altman method, we derived the rate expression for Scheme 3:

$$\frac{v}{[E]_T} = \frac{k_3}{\frac{k_4(k_{-2}+k_3)}{k_2k_5[O_2][P]} + \frac{k_{-2}+k_3}{k_2[O_2]} + 1 + \frac{k_3}{k_1[L]} + \frac{k_4(k_{-2}+k_3)}{k_1k_2[L][O_2]}} \quad \text{(A1)}$$

Under conditions where the concentration of L goes to infinity

$$\frac{v}{[E]_T} = \frac{k_3}{\frac{k_4(k_{-2}+k_3)}{k_2k_5[O_2][P]} + \frac{k_{-2}+k_3}{k_2[O_2]} + 1} \quad \text{(A2)}$$

Rearranging eq A2, and noting that the rate of turnover is equal to $k_{cat}/K_M(O_2)[O_2]$, leads to a simplified form

$$\frac{v}{[E]_T} = \frac{k_{cat}}{K_M(O_2)}[O_2] = \frac{k_2k_3[O_2]}{(k_{-2}+k_3)\left(\frac{k_4}{k_5}\frac{1}{[P]} + 1\right)} \quad \text{(A3)}$$

It can be seen that the denominator simplifies to ($k_{-2} + k_3$) in the limit of saturating [P], leading to the Michaelis−Menten equation, with $K_M(O_2) = (k_{-2} + k_3)/k_2$. However, for finite [P] $K_M(O_2)$ is more complicated. Making the substitution $K_M(O_2) = (k_{-2} + k_3)/k_2$ leads to the following relationship for $k_{cat}/K_M(O_2)$ as a function of [P]:

$$\left(\frac{k_{cat}}{K_M(O_2)}\right)_{obs} = \frac{\left(\frac{k_{cat}}{K_M(O_2)}\right)_{max}}{\left(\frac{k_4}{k_5}\frac{1}{[P]}\right) + 1} = \frac{\left(\frac{k_{cat}}{K_M(O_2)}\right)_{max}}{\frac{K_A}{[P]} + 1} \quad \text{(A4)}$$

Making the substitution $K_A = k_4/k_5$ converts eq A4 into the form used within the text. It can be seen that the apparent $k_{cat}/K_M(O_2)$ has a hyperbolic dependence on [P] and that the half-maximal $k_{cat}/K_M(O_2)$ is observed when [P] = K_A. K_A has the units of concentration and represents the ratio of the rate of L$^\bullet$ loss from E (k_4) to the second-order rate constant for P reactivating E (k_5). When [P] ≫ K_A, all enzyme is in the active form (E*, or Fe^{3+}−OH), as k_5[P] ≫ k_4 under this condition. Conversely, when [P] ≪ K_A, enzyme accumulates in the inactive pool (E, or Fe^{2+}−OH_2), as k_5[P] ≪ k_4. Thus, the observed $k_{cat}/K_M(O_2)$ is a function of the partitioning of enzyme between the active and inactive pools.

REFERENCES

1. Gardner, H. W. (1989) *Biochim. Biophys. Acta 1001*, 274−281.
2. Samuelsson, B., Dahlen, S.-E., Lindgren, J., Rouzer, C. A., and Serhan, C. N. (1987) *Science 237*, 1171−1176.
3. Rioux, N., and Castonguay, A. (1998) *Carcinogenesis 19*, 1393−1400.
4. References therein ref *3*.
5. Kuhn, H. (2000) *Prostaglandins Lipid Mediat. 62*, 255−270.
6. Brash, A. R. (1999) *J. Biol. Chem. 274*, 23679−23682.
7. Minor, W., Steczko, J., Stec, B., Otwinowski, Z., Bolin, J. T., Walter, R., and Axelrod, B. (1996) *Biochemistry 35*, 10687−10701.
8. Boyington, J. C., Gaffney, B. J., and Amzel, L. M. (1993) *Science 260*, 1482−1486.
9. Steczko, J., Donoho, G. A., Dixon, J. E., Sugimoto, T., and Axelrod, B. (1991) *Protein Expression Purif. 2*, 221−227.

10. Holman, T. R., Zhou, J., and Solomon, E. I. (1998) *J. Am. Chem. Soc. 120*, 12564−12572.
11. Brash, A. R., Boeglin, W. E., Chang, M. S., and Shieh, B. H. (1996) *J. Biol. Chem. 271*, 20949−20957.
12. Gan, Q. F., Browner, M. F., Sloane, D. L., and Sigal, E. (1996) *J. Biol. Chem. 271*, 25412−25418.
13. Sloane, D. L., Leung, R., Craik, C. S., and Sigal, E. (1991) *Nature 354*, 149−152.
14. Schwarz, K., Borngraber, S., Anton, M., and Kuhn, H. (1998) *Biochemistry 37*, 15327−15335.
15. Gillmor, S. A., Villasenor, A., Fletterick, R., Sigal, E., and Browner, M. F. (1997) *Nat. Struct. Biol. 4*, 1003−1009.
16. Glickman, M. H., and Klinman, J. P. (1996) *Biochemistry 35*, 12882−12892.
17. Scarrow, R. C., Trimitsis, M. G., Buck, C. P., Grove, G. N., Cowling, R. A., and Nelson, M. J. (1994) *Biochemistry 33*, 15023−15035.
18. Tomchick, D. R., Phan, P., Cymborowski, M., Minor, W., and Holman, T. R. (2001) *Biochemistry 40*, 7509−7517.
19. Glickman, M. H., and Klinman, J. P. (1995) *Biochemistry 34*, 14077−14092.
20. Jonsson, T., Glickman, M. H., Sun, S. J., and Klinman, J. P. (1996) *J. Am. Chem. Soc. 118*, 10319−10320.
21. Nelson, M. J., Seitz, S. P., and Cowling, R. A. (1990) *Biochemistry 29*, 6897−6903.
22. Mims, M. P., Porras, A. G., Olson, J. S., Noble, R. W., and Peterson, J. A. (1981) *J. Biol. Chem. 258*, 14219−14232.
23. Nelson, M. J., Cowling, R. A., and Seitz, S. P. (1994) *Biochemistry 33*, 4966−4973.
24. Skrzypczak-Jankun, E., Bross, R. A., Carroll, R. T., Dunham, W. R., and Funk, M. O. (2001) *J. Am. Chem. Soc. 123*, 10814−10820.
25. Klinman, J. P. (2001) *J. Biol. Inorg. Chem. 6*, 1−13.
26. Schwartz, B., Dove, J. E., and Klinman, J. P. (2000) *Biochemistry 39*, 3699−3707.
27. Francisco, W. A., Merkler, D. J., Blackburn, N. J., and Klinman, J. P. (1998) *Biochemistry 37*, 8244−8252.
28. Francisco, W. A., Tian, G. C., Fitzpatrick, P. F., and Klinman, J. P. (1998) *J. Am. Chem. Soc. 120*, 4057−4062.
29. Glickman, M. H., Cliff, S., Thiemens, M., and Klinman, J. P. (1997) *J. Am. Chem. Soc. 119*, 11357−11361.
30. Stahl, S. S., Francisco, W. A., Merkx, M., Klinman, J. P., and Lippard, S. J. (2001) *J. Biol. Chem. 276*, 4549−4553.
31. Su, Q. J., and Klinman, J. P. (1999) *Biochemistry 38*, 8572−8581.
32. Su, Q. J., and Klinman, J. P. (1998) *Biochemistry 37*, 12513−12525.
33. Tian, G. C., Berry, J. A., and Klinman, J. P. (1994) *Biochemistry 33*, 14650−14650.
34. Knapp, M. J., Seebeck, F. P., and Klinman, J. P. (2001) *J. Am. Chem. Soc. 123*, 2931−2932.
35. Goto, Y., and Klinman, J. P. (2002) *Biochemistry 41*, 13637−13640.
36. Roth, J., and Klinman, J. P. (2003) *Proc. Natl. Acad. Sci. U.S.A. 100*, 62−67.
37. Rickert, K. W., and Klinman, J. P. (1999) *Biochemistry 38*, 12218−12228.
38. Nelson, M. J., and Cowling, R. A. (1990) *J. Am. Chem. Soc. 112*, 2820−2821.
39. Whittaker, J. W., Orville, A. M., and Lipscomb, J. D. (1990) *Methods Enzymol. 188*, 82−88.
40. Gevantman, G. H. (1987) in *CRC Handbook of Chemistry and Physics* (Lide, D. R., Ed.) pp 8−87, CRC Press, Boca Raton, FL.
41. KaleidaGraph, Synergy Software.
42. Fersht, A. (1985) *Enzyme Structure and Mechanism*, 2nd ed., W. H. Freeman, New York.
43. Tian, G. C., and Klinman, J. P. (1993) *J. Am. Chem. Soc. 115*, 7117−7127.
44. Hasinoff, B. B., and Chishti, S. B. (1982) *Biochemistry 21*, 4275−4278.
45. Hardy, L. H., and Kirsch, J. F. (1984) *Biochemistry 23*, 1275−1282.
46. Schilstra, M. J., Veldink, G. A., Verhagen, J., and Vliegenthart, J. F. G. (1992) *Biochemistry 31*, 7692−7699.
47. DeGroot, J. J. M. C., Veldink, G. A., Vliegenthart, J. F. G., Boldingh, J., Wever, R., and Van Gelder, B. F. (1975) *Biochim. Biophys. Acta 377*, 71−79.
48. Schilstra, M. J., Veldink, G. A., and Vliegenthart, J. F. G. (1994) *Biochemistry 33*, 3974−3979.
49. Berry, H., Debat, H., and Garde, V. L. (1998) *J. Biol. Chem. 273*, 2769−2776.
50. The work by Berry et al. fixed $k_4 = 2.3 \times 10^3\ s^{-1}$, which lead them to estimate the rate of $H^{\bullet}$ abstraction as $31 \times 10^3\ s^{-1}$, yet this rate has been measured by many workers as ca. $300\ s^{-1}$.
51. Ludwig, P., Holzhütter, H.-G., Colosimo, A., Silvestrini, M. C., Schewe, T., and Rapoport, S. M. (1987) *Eur. J. Biochem. 168*, 325−337.
52. Blacklow, S. C., Raines, R. T., Lim, W. A., Zamore, P. D., and Knowles, J. R. (1988) *Biochemistry 27*, 1158−1167.
53. Bazelyansky, M., Robey, E., and Kirsch, J. F. (1986) *Biochemistry 25*, 125−130.
54. Nelson, M. J. (1987) *J. Biol. Chem. 262*, 12137−12142.
55. Pavlosky, M. A., and Solomon, E. I. (1994) *J. Am. Chem. Soc. 116*, 11610−11611.
56. Klinman, J. P. (1978) *Adv. Enzymol. Relat. Areas Mol. Biol. 46*, 415−494.
57. Page, C. C., Moser, C. C., Chen, X. X., and Dutton, P. L. (1999) *Nature 402*, 47−52.
58. Grissom, C. B. (1995) *Chem. Rev. 95*, 3−24.
59. Knapp, M. J., Rickert, K., and Klinman, J. P. (2002) *J. Am. Chem. Soc. 124*, 3865−3874.
60. Browner, M. F., Gillmor, S. A., and Fletterick, R. (1998) *Nat. Struct. Biol. 5*, 179.
61. Prigge, S. T., Gaffney, B. J., and Amzel, L. M. (1998) *Nat. Struct. Biol. 5*, 178−179.
62. In the L29W mutant of sperm whale myoglobin, kinetic barriers of ca. 2 kcal/mol have been observed between states in which CO is unbound to heme Fe and the bound Fe−CO state. See ref *64*.
63. Chu, K., Vojtchovsky, J., McMahon, B. H., Sweet, R. M., Berendzen, J., and Schlichting, I. (2000) *Nature 403*, 921−923.
64. Ostermann, A., Waschipky, R., Parak, F. G., and Nienhaus, G. U. (2000) *Nature 404*, 205−208.
65. Scott, E. E., and Gibson, Q. H. (1997) *Biochemistry 36*, 11909−11917.
66. Tilton, R. F., Jr., Kuntz, I. D., Jr., and Petsko, G. A. (1984) *Biochemistry 23*, 2849−2857.
67. Bowers, C. R., Storhaug, V., Webster, C. E., Bharatam, J., Cottone, A., Gianna, R., Betsey, K., and Gaffney, B. J. (1999) *J. Am. Chem. Soc. 121*, 9370−9377.

BI0300884